

# A picometer-accuracy, laser-metrology gauge for Keck Interferometer differential-phase subsystem

Yekta Gürsel

Jet Propulsion Laboratory, California Institute of Technology, Pasadena, California, U.S.A.

## ABSTRACT

Keck Interferometer differential-phase planet-detection system requires a picometer accuracy, large ( $2\ \mu\text{m}$  to  $4\ \mu\text{m}$ ) amplitude optical path-length modulator that can operate at fairly high frequencies (250 Hz, 750 Hz, and 1250 Hz, a partial, triangular wave motion).

We have developed a gauge which monitors the amplitude of the motion of the path-length modulator and which is capable of reaching a sensitivity of at least  $3\ \text{pm}$  per  $\sqrt{\text{Hz}}$  within a band width of 1 Hz at 250 Hz, 750 Hz, and 1250 Hz. Two of these gauges are built. The gauges are compared to each other while monitoring a common optical path-length modulator to determine their accuracy.

In this paper, the gauge construction details, the results of the gauge accuracy tests as well as the final path-length modulator performance details are presented.

**Keywords:** Ground-based interferometry, planet detection, differential phase

## 1. INTRODUCTION

The Keck Interferometer<sup>1</sup> combines the light input from the two 10-m Keck telescopes across a baseline of 85 m. One of the goals of this interferometer is to detect extra-solar planets orbiting distant stars.

A particular way to detect these planets is to interferometrically track the star-planet system while making observations of the interferometric phase at several wavelengths at once. Since the light from the planet has a spectral distribution different from that of the parent star, the difference in the detected interferometric phase between different wavelengths is a function of the apparent star-planet separation.<sup>2</sup>

The intensity of the light from the planet is many orders of magnitude smaller than the intensity of the light emitted by the parent star. As a result, the interferometric differential phase measurements have to be very accurate to distinguish the star-planet signal from the instrument noise.

A common way to measure interferometric phase is to change the interferometric path-length difference by precise amounts while recording the interferometric fringe intensity.<sup>2</sup> The phase can then be de-convolved from this series of intensity measurements. This method is known as phase-shifting interferometry as the interferometric phase changes linearly with the changing optical path-length.

The device that changes the optical path-length in an interferometer is the path-length modulator. The path-length modulator serves two different purposes. One is to change the path-length by precisely known amounts, and the other is to modulate the path-length rapidly so that a synchronous detection of the interferometric phase can be made to avoid the effects of atmospheric turbulence and ground-induced vibrations.

The path-length modulator is constructed by placing a retro-reflector on a linear, magnetic drive. The starlight bounces off the retro-reflector as it moves back and forth modulating the phase of the light that reflects from it, proportional to its wavelength and the amplitude of the retro-reflector motion. The motion of the retro-reflector has to be monitored very precisely in order to be able to deconvolve the interferometric phase with sufficient accuracy to detect the differential phase signal created by the star-planet system.

---

Further author information:

E-mail: Yekta.Gursel@jpl.nasa.gov, Telephone: 1 818 354 3645, Address: Mail Stop 306-388, Jet Propulsion Laboratory, 4800 Oak Grove Dr., Pasadena, CA, 91109, U.S.A.

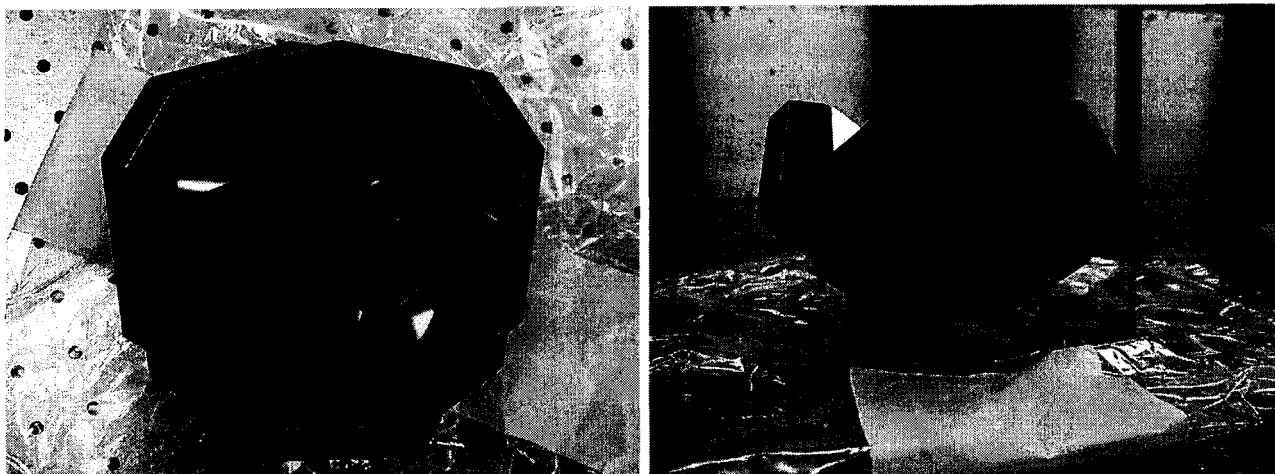


**Figure 1.** Left: Path-length modulator retro-reflector cube. Right: Side view with the gauge pick-off and the flexure mount.

We have developed a path-length modulator and a gauge which monitors the amplitude of the motion of the path-length modulator and which is capable of reaching a sensitivity of at least  $3 \text{ pm per } \sqrt{\text{Hz}}$  within a band width of 1 Hz at 250 Hz, 750 Hz, and 1250 Hz. Two of these path-length modulators and gauges are built. The gauges are compared to each other while monitoring a common optical path-length modulator to determine their accuracy.

In what follows, the path-length modulator and the gauge construction details, the results of the gauge accuracy tests as well as the final path-length modulator performance details are presented.

## **2. THE PATH-LENGTH MODULATOR**

The path-length modulator consists of three parts: The retro-reflector that reflects the starlight back without severely altering its wavefront quality, the gauge pick-off that returns the gauge probe beam to the gauge for amplitude measurements while supplying an alignment beam that is used to align the starlight parallel to the retro-reflector motion, and a linear, magnetic driver which moves the retro-reflector and pick-off assembly with the required amplitudes at the required frequencies without imparting excessive vibrations into the instrument due to its own motion.

### **2.1. The retro-reflector**

A 127 mm clear aperture, fused-quartz, gold-coated, hollow corner-cube is used as the retro-reflector. The advantages of using a straight retro-reflector instead of a cat's-eye type delay line are many fold: The reflected beam does not go through a focus, avoiding the cat's-eye's problem of changing the focus while changing the path-length. The mechanical structure of the entire system is much simpler, consisting of one solid optical piece as opposed to several optical pieces held together with metal rods and other arrangements in a cat's-eye.

The retro-reflection accuracy of the cube is 1 arc-second. The starlight beam only reflects from the sides of the retro-reflector, without contacting the areas where the adjacent faces join. This arrangement prevents the starlight beam wavefront from being severely distorted due to the joining lines.<sup>3</sup>

The total amount of wavefront distortion across the clear aperture in the configuration described above is 0.4 waves at 633 nm. This translates to a wavefront distortion of about 0.1 waves at the operating wavelength of 2200 nm. The cube with its mount weighs about one kilogram, and it is designed to take forces up to 8 N continuously at 250 Hz, 750 Hz, and 1250 Hz.

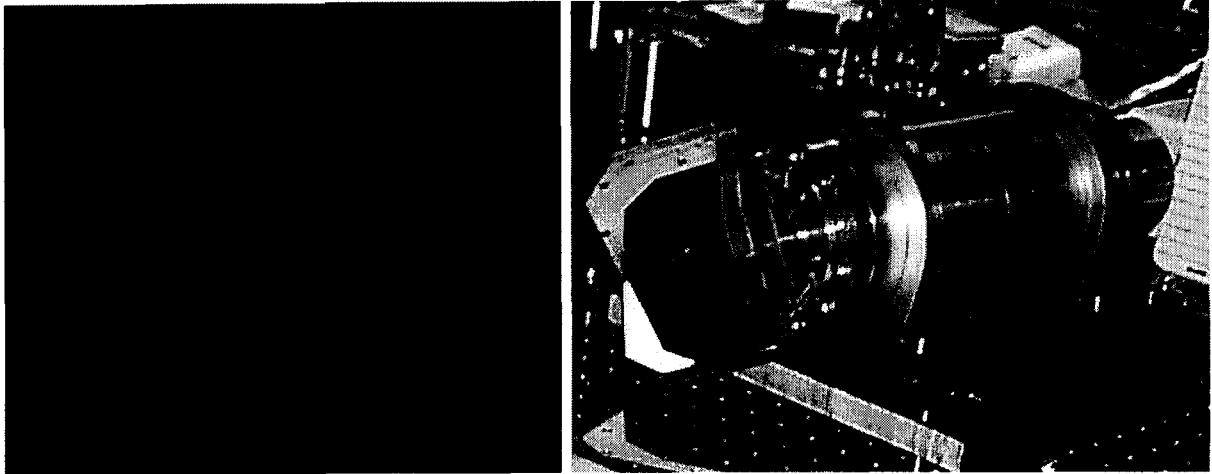


**Figure 2.** Left: Actual retro-reflector and pick-off alignment pattern. Right: Retro-reflector and counter weight on the modulator driver.

Fig. 1 shows a picture of one of the cubes looking straight into it and a picture of the side view of the same cube with its mount and the pick-off. The corner of the cube where all three faces join is ground-off, and the gauge pick-off with its reflective side facing away and coinciding with the ground-off optical corner is glued to cover the resulting triangular hole. The optical clear-aperture through the triangular hole is 5 mm. The pick-off itself reflects impinging light back in the shape of a triangle, whereas the cube reflects a perfect hexagon back, due to reflection from all three sides. The resulting exactly centered triangle in a perfect hexagon pattern when the retro-reflected beam from the cube is parallel to the beam reflected-off from the pick-off is designed purposely to aid in alignment.

## 2.2. The gauge pick-off

The gauge pick-off is a 1" diameter, 0.250" thick, fused-quartz substrate with a 3 arc-minute wedge. Both surfaces are polished flat to  $\lambda/10$  at 633 nm, and the surface facing away from the cube is coated with a 90% reflection, 10% transmission at 0 degree angle of incidence at 633 nm, dielectric coating. The surface facing toward the cube is coated with a super-V anti-reflection coating with a maximum reflected intensity ratio of 0.05% at 633 nm at 0 degree angle of incidence.

The pick-off is glued to the cube in such a way to bring the reflective surface within 100  $\mu\text{m}$  of the optical cube corner, with the reflective surface perpendicular to the cube axis within a few arc-minutes.

## 2.3. The modulator driver

The modulator-driver is a one-dimensional, voice-coil motion element, with dual stainless-steel membranes with pre-load that supplies the linear restoring force, which confine the motion to a single degree of freedom. The driver has two such independent units at opposing ends moving simultaneously in opposite directions.

One end of the modulator holds the retro-reflector cube, while the other end carries a precisely matched counter-weight to cancel any linear momentum during the operation resulting in no-vibration transfer to the rest of the instrument. The voice coils which are capable of generating 80 N of force each are driven individually by a Techron 7520 stereo amplifier. Most of this force is used to fight the restoring force of the dual membranes.

A 3/8" hole runs through the counter-weight, the membranes, the voice-coils and the modulator driver housing to supply rear-access to the retro-reflector gauge pick-off mirror. The cube is mounted to the modulator driver by a triple invar flexure with fused-quartz pads at the cube and invar stand-offs at the modulator end. The stand-offs mount to a ring and the ring mounts to the modulator driver through another thin ring which prevents stress induced deformations. Fig. 2 shows the cube alignment pattern and one of the cubes mounted on one of the modulator drivers.

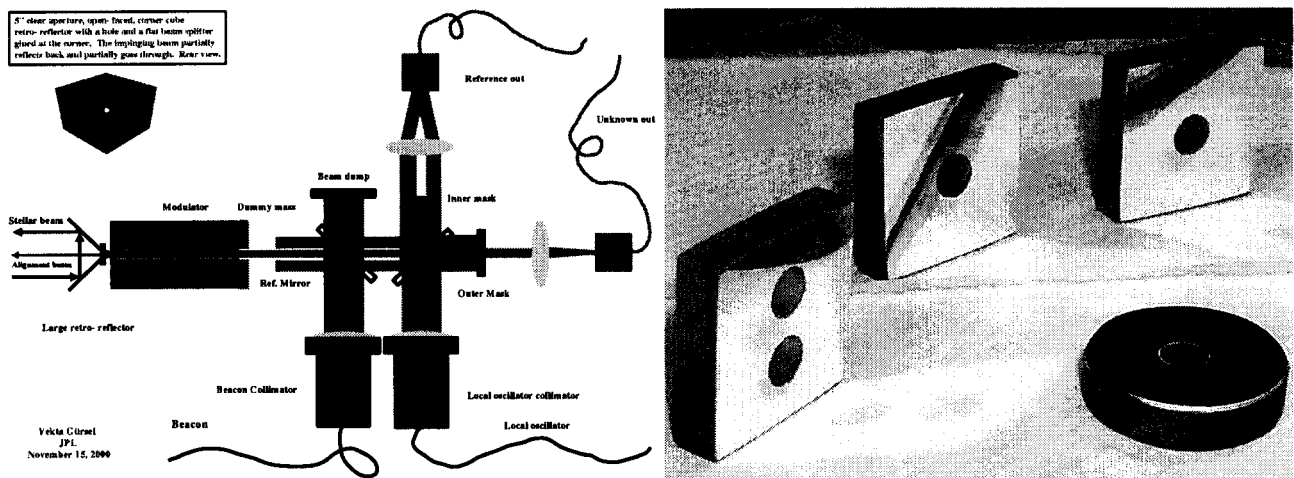


**Figure 3.** Left: Path-length modulator amplitude measurement system. Right: The reference-beam-probe-beam beam separator-combiner mirrors.

### 3. THE GAUGE

The gauge design is schematically shown in Fig. 3. It is similar to one of the designs considered for Space Interferometry Mission (SIM)<sup>4,5,6</sup> but with vast optical improvements.

The gauge is a polarization-insensitive heterodyne gauge which consists of matched collimators, photo-diode receivers, and beam separators. It is fed by a heterodyne plate that uses a Spectra Physics Model 117A stabilized He-Ne laser to supply four, fiber-coupled laser beams which are pairwise 80 kHz apart in frequency to feed two heterodyne gauges.

#### 3.1. The matched collimators and the photo-diode receivers

The matched collimators are made out of an angle polished polarization maintaining fiber and a 50 mm diameter, 120.2 mm focal length, super-V coated at 633 nm, achromatic lens mounted in a blackened aluminum tube with all internal threads. The threads serve as light baffles against scattered light. A shear plate is used to bring the system to collimation and the entire collimator is permanently glued up at this point leaving no adjustments to perform.

The wavefront coming out of the collimators is not very flat, only a few fractions of the wavelength at 633 nm. However, they match each other very well. In order to test this, two collimator outputs are combined by a beam splitter and both ports of the beam splitter were monitored by a phase sensitive detector. The apertures of the collimators are then changed while monitoring the phase changes in the output beam. When one of the collimators is at half of the total power aperture and the other one is at 0.25 of the total power aperture (6.75 mm), the total phase shift due to the wavefront mismatch between the two is 1.784 nm. This is match that is better than  $\lambda/350$  at 633 nm. The gauge apertures are set near these values to guarantee the wavefront match.

The photo-diode receivers are built like the inverse matched collimators. Same lens in the same mechanical arrangement is used. The 100  $\mu\text{m}$  diameter sensitive area photo-diode is mounted at the precise focal point of the focusing lens, at nearly the same angle as that of the angle polished fiber. The whole arrangement is then glued permanently leaving no adjustments to perform. The photo-diode pre-amplifier and the cable-driver are built right into the focuser body and thoroughly shielded to eliminate any electrical interference.

The small area detector is one of the main improvements of this gauge design. Since gauge design uses inner and outer masked beams, the leakage between these two beams is due to diffraction. However, the diffracted leakage travels at a slight angle to the main un-diffracted beam. The precise focal point placement causes these diffracted parts to be sent elsewhere on the focal plane and small area of the photo-diode excludes them,

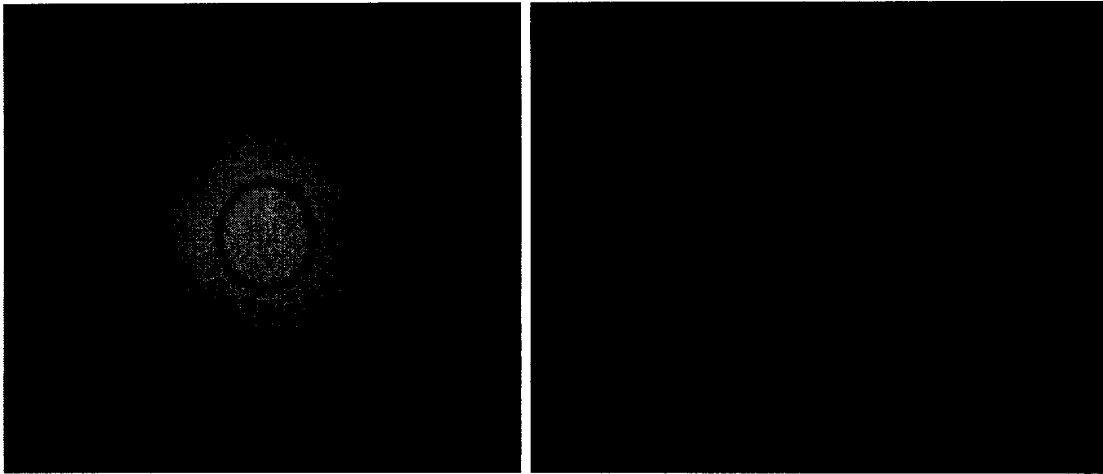


**Figure 4.** Left: The combined reference beam and returning probe beam after the probe-beam beam-separator mirror. Right: The probe and reference beam fringes just before separation.

picking up only the uncontaminated beam. The tilt of the photo-diode with respect to the main beam causes the unused part of the detected beam to travel away from the photo-detector and to get absorbed by the blackened, threaded focuser body.

### 3.2. The beam separators

The beam separators are either mirrors with holes drilled into them, or masks that block certain parts of a beam before it reaches a photo-receiver. A particular example of this is the reference-unknown beam separator mirror at the optical probe beam output of the gauge. These mirrors are made by simply drilling a hole into an existing mirror. The hole diameter is critically chosen to maintain the wavefront match and to supply a natural separation between the returning probe beam and the reference beam. This is another major improvement to the gauge that reduces the systematic error.

Fig. 3 shows some of the drilled reference mirrors with the critical hole diameters chosen as explained. Fig. 4 show the combined beam formed by the reflected beam from the probe-beam beam-separator mirror and the returning probe beam passing through the same mirror. A dark band clearly separates the inner and outer parts of the combined beam reducing the systematic error.

### 3.3. Internal gauge alignment

The gauge systematic errors are also caused by the reference and the probe beams returning to the probe collimator and coupling back into the fiber. Since the collimators are built like the photo-receivers, a slight angle in the return beams will cause them to be mapped elsewhere on the collimator focal plane avoiding the interference. This is possible as only the returning probe collimator beams and local oscillator beam have to overlap, not the initial probe collimator beam. Furthermore, the local oscillator beam combiner can be placed to prevent any beam from getting into the local oscillator fiber. The gauge is aligned to satisfy both of these constraints.

Fig. 5 shows one of the aligned gauges. It is built on a 12" x 24" x 2" optical breadboard and it is transportable without losing alignment.

Fig. 4 shows the gauge fringes at DC with heterodyne modulation turned off just before they enter the photo-receivers. Both beams are tilted slightly to make the fringes more visible. The gauge normally operates at "0-fringe" for maximum signal-to-noise ratio.

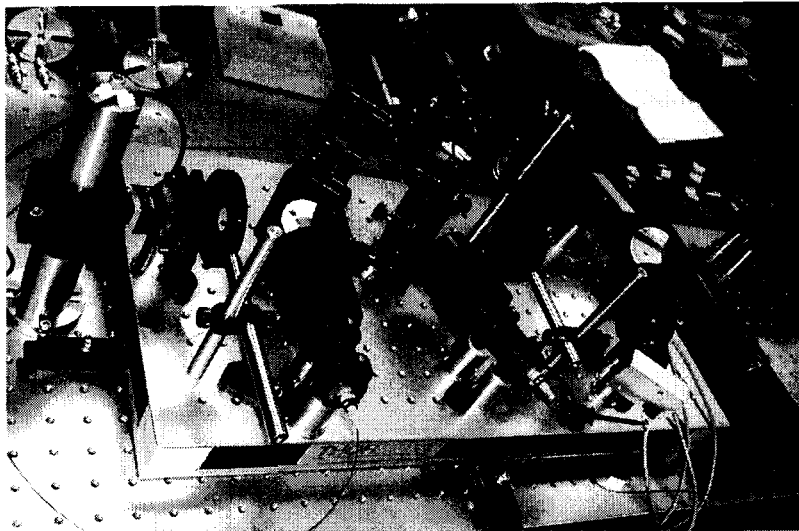


Figure 5. The assembled differential phase path-length-modulator amplitude monitor gauge.

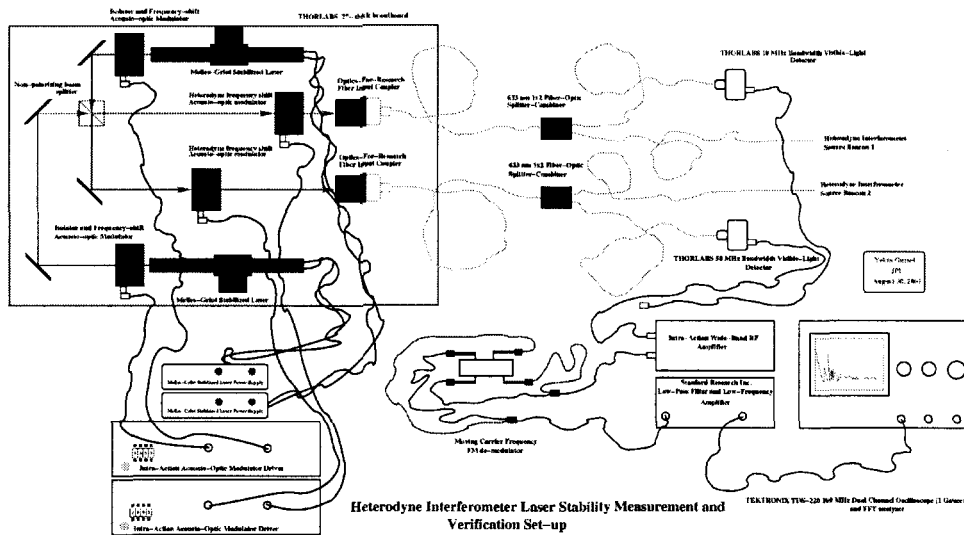
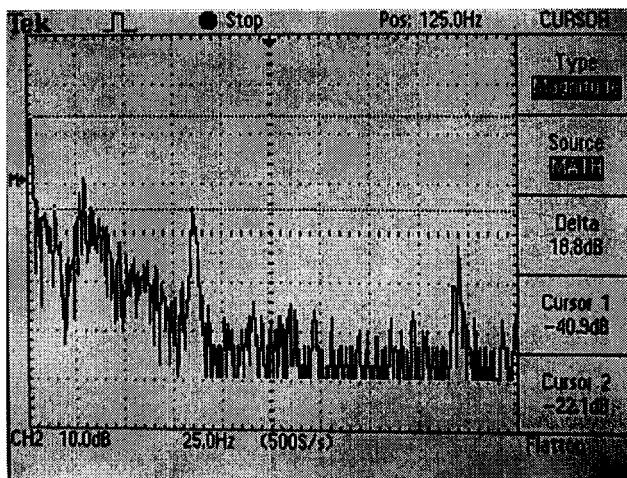
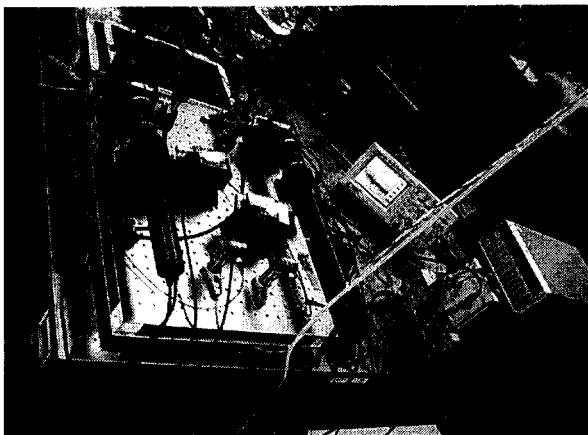


Figure 6. The diagram of the fully-populated heterodyne plate.

### 3.4. The heterodyne plate

The heterodyne plate generates the two fiber-coupled laser beams that are 80 kHz apart in frequency from a stabilized laser to feed the heterodyne gauge. Since the gauge reference arm length is vastly shorter than the gauge probe arm length, any changes in the laser frequency show up as real distance change signals. To monitor the stability of the laser, the heterodyne plate has provisions to take another laser and optically beat the two lasers together to monitor the laser frequency changes.

Fig. 6 shows a diagram of the fully populated heterodyne plate. The lasers themselves are protected from back-reflections by separate acousto-optic modulators that also help in making the frequency difference between them smaller or larger. The plate can beat two lasers together while running a heterodyne gauge or it can run two heterodyne gauges simultaneously. The beat laser is blocked in the latter case. Fig. 7 shows a picture of the actual heterodyne plate and the output of the FM demodulator that monitors the laser beat frequency. For



**Figure 7.** Left: The picture of the fully-populated heterodyne plate. Right: The frequency spectrum of the beat signal between two Spectra-Physics Model 117A lasers.

calibration, the peak at 5 Hz corresponds to a frequency change of 300 kHz rms per laser. The peak at 85 Hz corresponds to a frequency change of 40 kHz rms per laser.

### 3.5. The external gauge electronics and software

The signals produced by the photo-receivers are carried to the post-amplifiers with long shielded cables. The post-amplifiers convert the sinusoidal waveforms into square waves, and these square waves are fed into a phase digitizer which produce readings at precisely known intervals determined by a timing module. The entire system resides in a VME crate with a 333 MHz PowerPC single board CPU which performs the data recording.

All software is written by the author, and it is capable of recording a single gauge channel at 62,500 Hz, and two gauge channels at 31,250 Hz with time tags into memory simultaneously. The recordings are subsequently written to a networked, hard-disk data storage and backed up on CD-R's.

## 4. GAUGE TESTS

The gauges are tested for ambient noise level for very short absolute path-length differences, for noise level during scanning a few microns of path-length change for very short absolute path-length differences, and for systematic errors while two gauges are simultaneously monitoring the modulator driver with large absolute path-length differences.

### 4.1. Ambient noise level tests

To determine the internal gauge noise level, the probe beam output mirror is replaced with a mirror without a hole. A recording of the gauge output is made at 62,500 Hz for 57 seconds. Fig. 8 shows the magnitude of the fourier transform of the one-way path-length change monitored by one of the gauges. The plot is calibrated like an AC voltmeter: Any peak that is exactly on a bin of the fast-fourier-transform output will show the actual amplitude of the signal at that frequency.

The plethora of very narrow peaks in the spectrum justify this kind of calibration as their amplitude is directly readable. For example, the very sharp line peak at 60 Hz is barely reaching 1 pm amplitude. This proves that our shielding practices are excellent. The cluster of peaks at 5000 Hz seems to exist in almost every lab at JPL. Their source is still a mystery, although there are speculations that the power distribution units may be causing them.

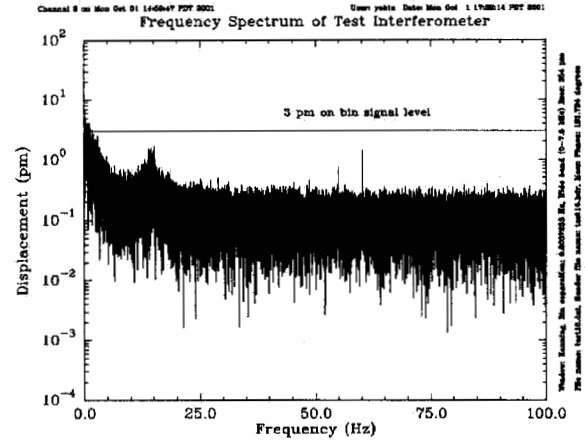
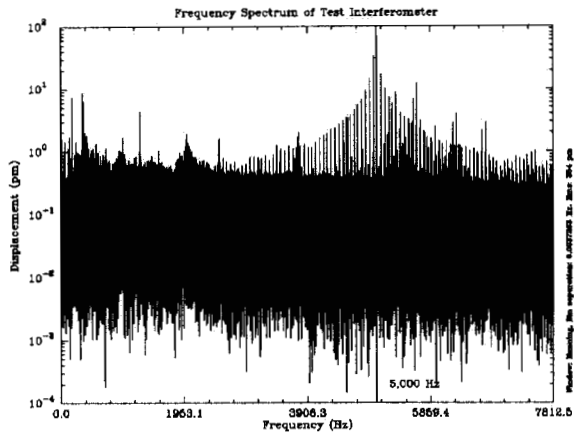


**Figure 8.** The magnitude of fourier transform of the one-way path-length change detected by one of the gauges with a common mirror.

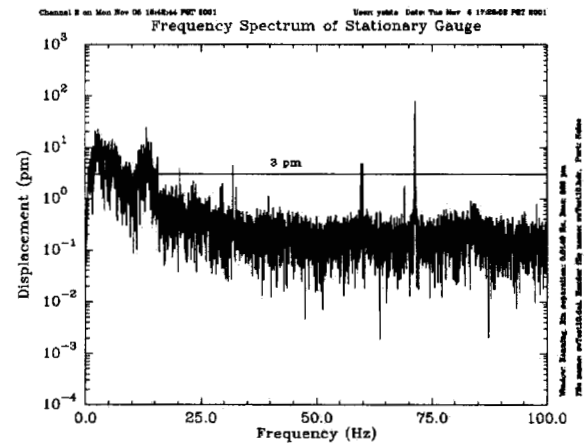
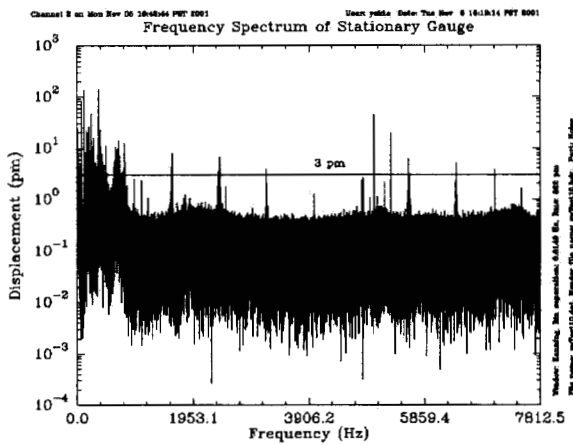


**Figure 9.** The magnitude of fourier transform of the one-way path-length change detected by one of the gauges with a stationary piezo-electric stage.

The gauge is then set up as shown in Fig. 5. A piezo-electric mirror is placed very close to the exit port for the probe beam resulting in a 30 mm absolute path-length difference. The mirror is not driven during these tests. Again, a recording is made at 62,500 Hz for 57 seconds.

The recording shows a drift as well as the noise, since the optical table and piezo-electric stage thermally expand during the recording. This 20 nm peak-to-peak, almost-linear drift is separated from the data with a long time-constant (2 s) low-pass filter.

Fig. 9 shows the magnitude of the fourier transform of the one-way path-length change monitored by one of the gauges in this case. There are more peaks and humps due to mechanical vibrations in the spectra, but the gauge still easily meets the quietness requirement at 250 Hz, 750 Hz, and 1250 Hz, and at most other places in the spectrum. Note that the peak at 60 Hz is larger. This is due to actual mechanical shaking as it will be proved in the two-gauge tests.

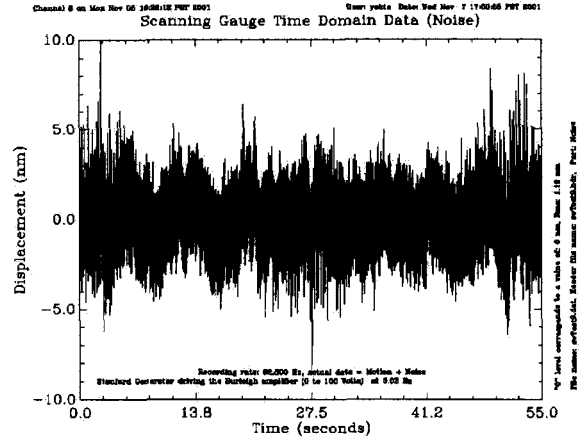
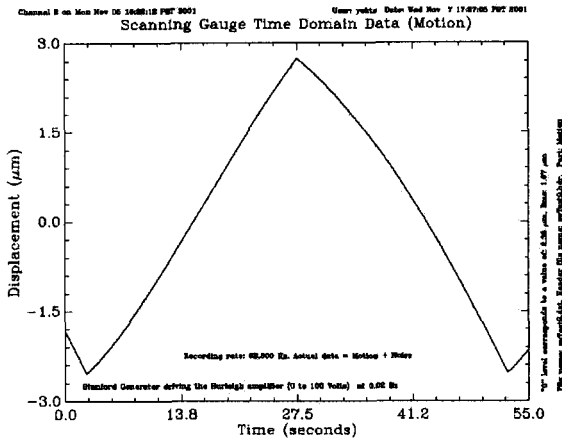


**Figure 10.** The magnitude of fourier transform of the one-way path-length change detected by one of the gauges with a stationary piezo-electric stage.

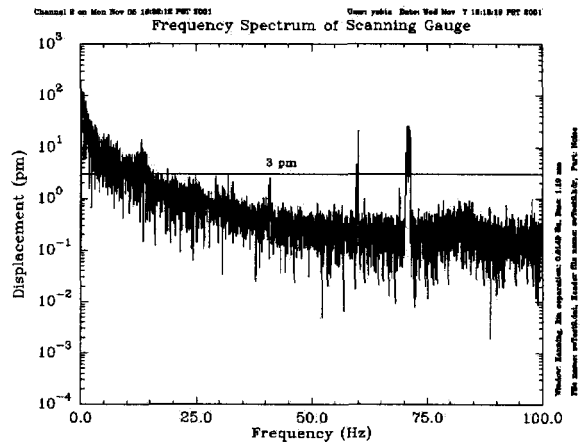
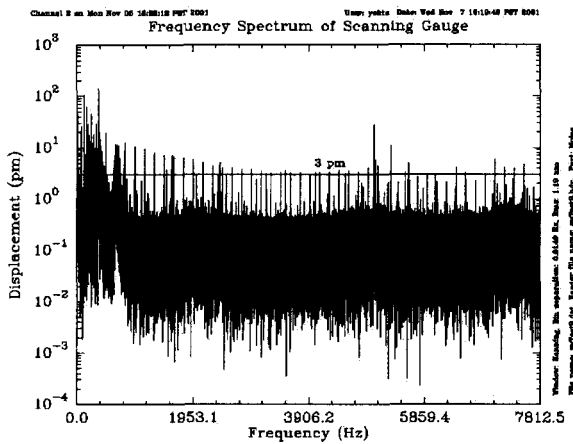


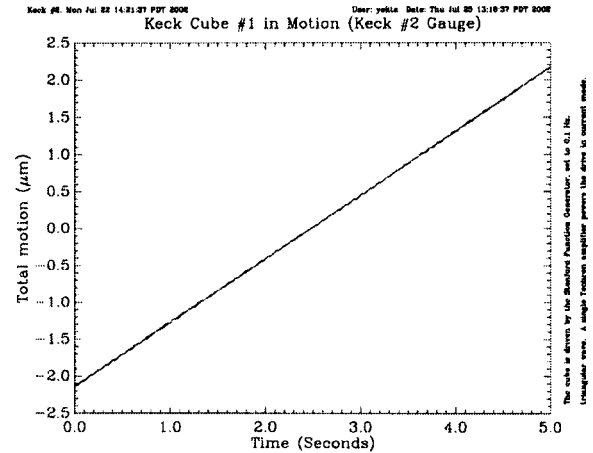
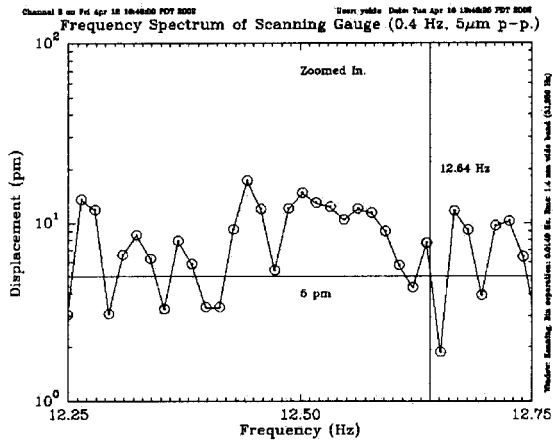
**Figure 11.** The magnitude of fourier transform of the one-way path-length change detected by one of the gauges with a stationary piezo-electric stage.

## 4.2. Scanning gauge tests

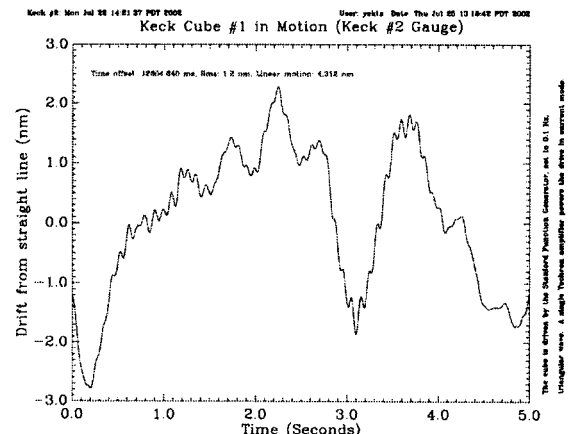
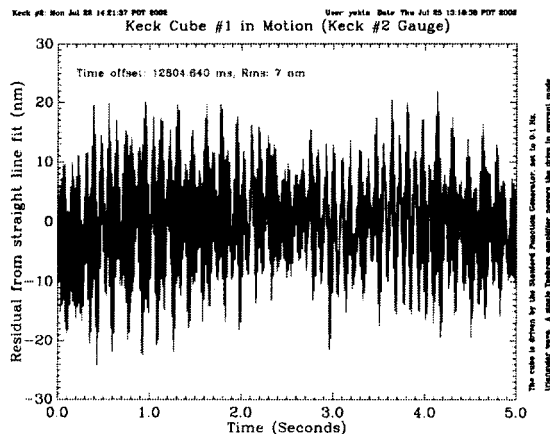
In the configuration described above, the piezo-electric stage is now driven by a triangular-wave generator through a high voltage amplifier. The three-channels of the piezo-electric stage are driven in a manner to make the mirror motion perpendicular to the probe beam.

Fig. 10 shows the two parts of the motion: The fitted slow part (a triangular wave with a period of 50 seconds), and the residual when the slow motion is subtracted. The total motion is the direct sum of these two curves. The non-linearity evident in the slow part of the motion is caused by the piezo-electric mirror stage, as it will be proved in the modulator drive tests.

Fig. 11 shows the magnitude of the fourier transform of the one-way path-length change monitored by one of the gauges in this case. There are a lot of spikes in the spectra. These are caused by the sharp corner of the triangular wave that does not completely subtract due to the noise. Again, the gauge still easily meets the



**Figure 12.** Left: The region in which the gauge systematic error appears in the magnitude of fourier transform of the one-way path-length change for the scanning gauge. Right: The modulator driver takes over the scanning.



**Figure 13.** Left: The modulator-driver motion residual from a straight line. Right: The high-frequency mechanical motion and air turbulence are filtered out of the residual on the left.

quietness requirement at 250 Hz, 750 Hz, and 1250 Hz, and at most other places in the spectrum. Note that the peak at 60 Hz is not growing any larger, but it is widening. This is again due to actual mechanical shaking as it will be proved in the two-gauge tests.

Another piece of information that can be extracted from single gauge scans is a value for the systematic error of the gauge. This error is periodic with optical fringe wavelength (one half the wavelength of the probing laser light). In a five micron scan in 25 seconds as shown above, this error will appear as a peak at 12.64 Hz. Fig. 12 shows this region for the scan values shown previously. There is no sharp peak at 12.64 Hz, however the spectrum goes consistently above 10 pm around this value. This behavior is caused by the noise around the corners of the triangular wave as it will be shown in the two gauge tests. The systematic error peak goes off the expected frequency and also widens by a few Hz. This plot shows that the total systematic error is about few tens of picometers in a single gauge.

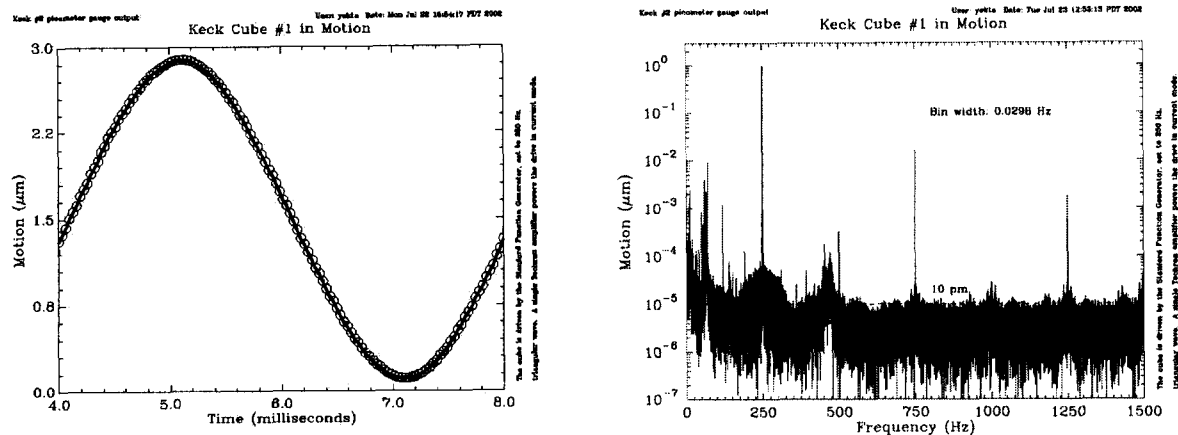


**Figure 14.** Left: The modulator-driver moving the retro-reflector at high frequency. Right: The magnitude of fourier transform of the one-way path-length change for the retro-reflector motion.

### 4.3. Modulator-driver motion linearity

The piezo-electric scanning mirror is replaced by our modulator driver next. The modulator driver is connected to Techron 7520 stereo power amplifier running in the current driver mode to cancel the drive coil self-inductance, driving the cube and the counter-weight simultaneously. During these tests, there is about 40 gm difference between the cube and the counter-weight. The counter-weight will be precisely balanced as the configuration approaches its final state.

The gauges are pointed to the gauge pick-off, and a recording is made to test the drive linearity. Fig. 12 shows the resulting motion as recorded by the gauge number 2. The difference between this curve and that produced by the piezo-electric driver is striking. Fig. 13 shows the residual from a straight line. Most of the residual is caused air-turbulence and mechanical vibrations. To make this clear, a low-pass filter was applied to the residual and the resulting curve still shows no indication of a non-linearity. It does look like low-frequency air turbulence. Note that the filtered residual has an rms value of 1.2 nm, out of a linear motion of 4,312 nm. We conclude that the drive is linear to at least 3 parts in 10,000 and it is almost certainly much better than this as the residual is random.

The drive frequency and waveform are brought closer to the actual drive frequency and the waveform in the differential phase set up for the next test. The resulting cube motion is shown in Fig. 14. The cube performs as expected, without sustaining any damage under continuous operating conditions. Although a perfect triangular-wave is applied to the Techron amplifier, the cube motion is closer to a sinusoidal waveform, as the flexure is operating above its resonance frequency. This will be rectified in the final configuration by a pre-distorted input to the amplifier. The frequency spectrum of this motion is shown in Fig. 14 and Fig. 15. Note that the peak at 60 Hz, is real mechanical motion as it will be proved in the next section. Fig. 15 also shows where the systematic error in the gauge will show up in this case. Again, there is a wide “hump” near the expected value just above 10 pm.

It is worthwhile to indicate that the Keck differential phase measurement is an AC coupled, synchronous measurement at 250 Hz, 750 Hz, and 1250 Hz in a 1 Hz bandwidth. The systematic error appears at a different frequency from these frequencies of interest. Under normal operating conditions, it will appear at a frequency higher than the highest frequency of interest (1250 Hz), and it does not effect any of the measurements as shown in Fig. 15. The systematic error is a concern only in DC measurements or in very wide-band AC measurements, like those needed by SIM.<sup>4</sup>

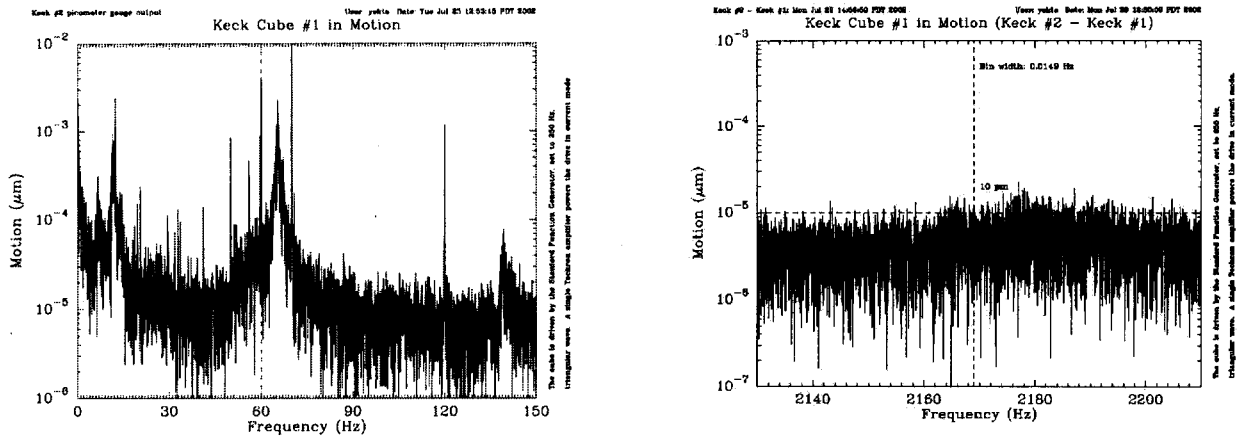


**Figure 15.** Left: The magnitude of fourier transform of the one-way path-length change for the retro-reflector motion. Right: The systematic error region for the retro-reflector motion.

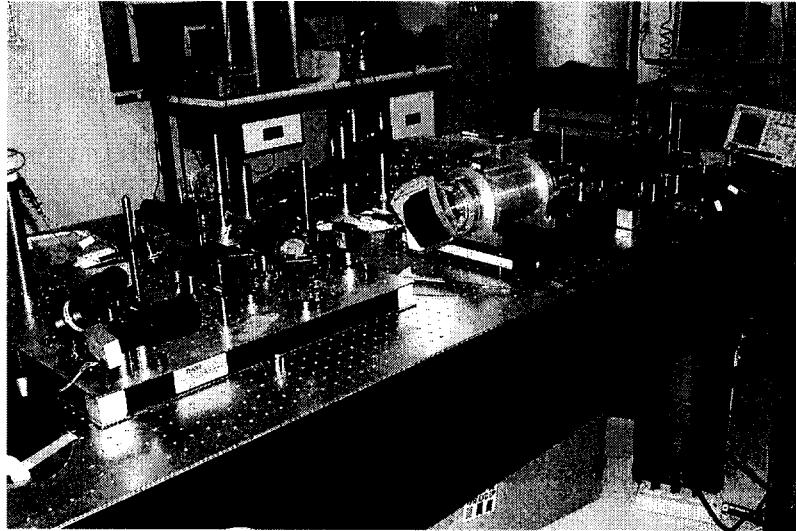


**Figure 16.** Both keck gauges are aligned to the retro-reflector pick-off mirror.

#### 4.4. Two gauge tests

In order to quantify the accuracy of the gauges, it is necessary to compare one of the gauges against the other while they track a common moving object. Two gauges are aligned to the pick-off mirror of the retro-reflector on the modulator-driver with the counter-weight as shown in Fig. 16.

Since the pick-off mirror is a flat beam splitter with 10% transmission, the probe beam of one gauge can interfere with the other gauge. This is prevented by switching the probe and the local oscillator frequencies in each gauge. This puts the probe beam of one gauge at the same frequency as that of the local oscillator of the other gauge, and causes an interfering signal at DC as both gauges are driven with the same laser. Since we are monitoring the heterodyne beat frequency at 80 kHz, the electronic filters completely stop the interference.

In this arrangement the absolute path-length differences are of the order of 1 m. Since the laser is stable to about 1 MHz per hour, it is possible that the laser frequency noise will affect the measurements. This is also

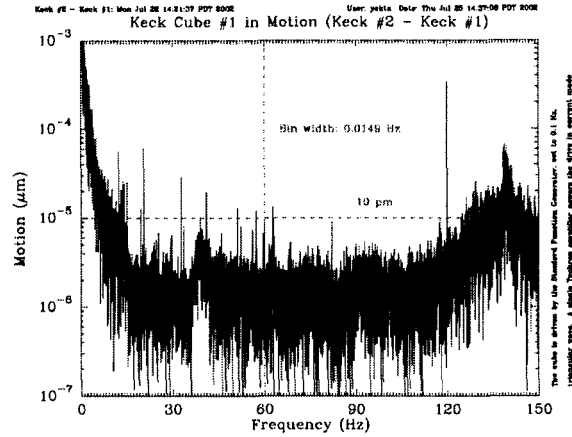
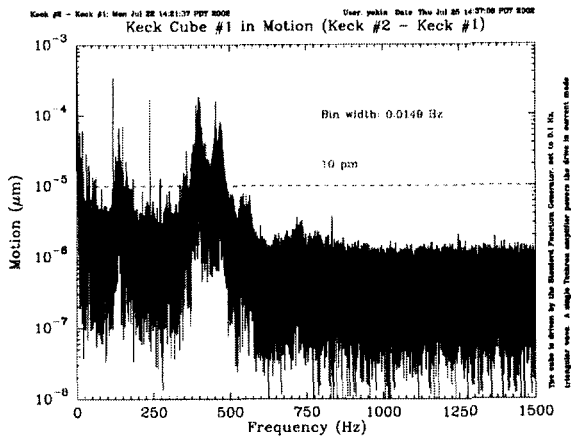


**Figure 17.** The magnitude of fourier transform of the difference between the two gauge readings of the one-way path-length change as they monitor the slowly moving retro-reflector.

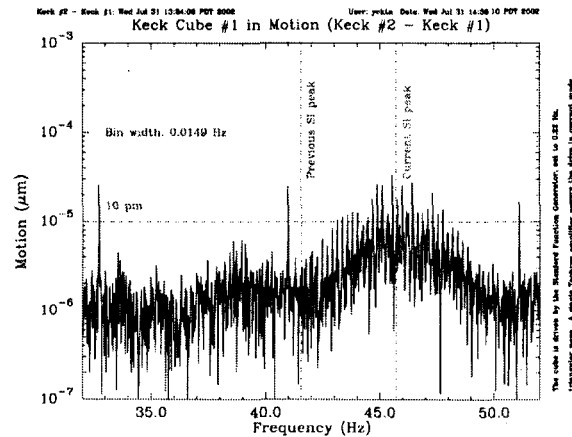
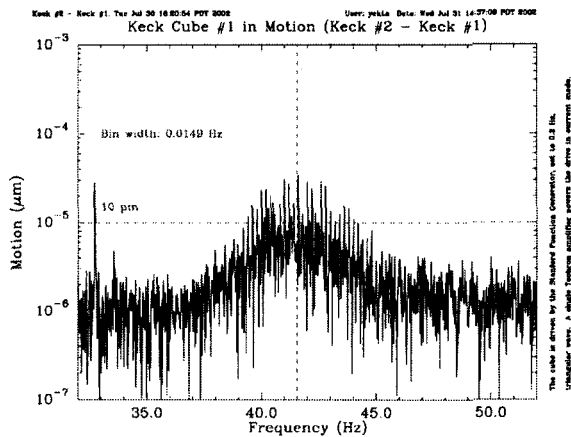


**Figure 18.** Left: The systematic error as it should appear in the gauge difference output for a particular motion amplitude. Right: The systematic error as it should appear in the gauge difference output when the motion frequency is increased by 10 percent.

avoided as the same laser drives both of the gauges and the laser frequency noise while appearing in each of the gauge's output, cancels out completely in the difference.

The systematic errors of the gauges, however, will not cancel out in general, and they will add-up in quadrature.

The spectra of the difference signal are shown in Fig 17 for a triangular-wave motion of the retro-reflector at a frequency of 0.2 Hz with a peak to peak amplitude of about 4.3  $\mu\text{m}$ . Note that all mechanical motions have been canceled out in the frequency band 20 Hz to 120 Hz. The peak at 120 Hz is almost certainly electrical pick-up, and the other very sharp spikes are likely to be acoustic noises that will be picked up differently by the gauges. The difference signal lies under 10 pm for all frequencies of interest, namely 250 Hz, 750 Hz, 1250 Hz. The wide hump around 300 Hz and above 125 Hz are the resonances of the individual mounts in the gauges. This is seen independently by loosening some of the mounts.

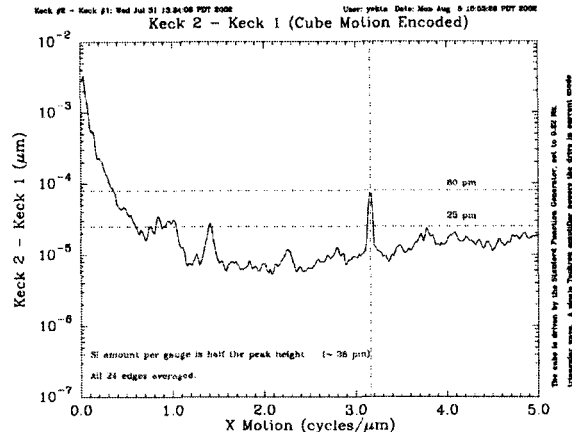
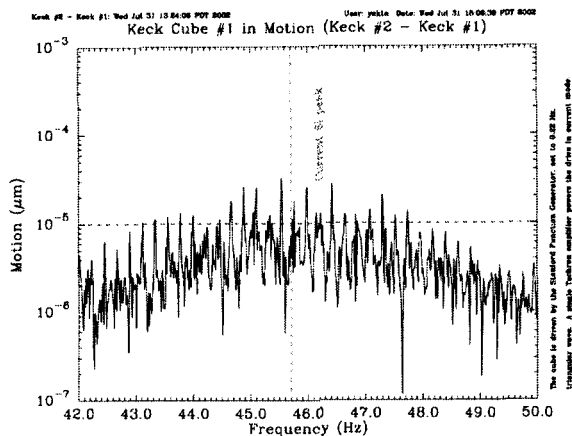


**Figure 19.** Left: The detailed look at the systematic error peak in the time domain. Right: The systematic error peak in the motion-encoded spatial domain using only the edges of the triangular-wave and averaging. Note the width of the peak and the lack of fine resolution.

Fig. 18 shows the systematic error peak in the difference signal. It is again a hump with many spikes. To make sure that this is the systematic error, the motion frequency is changed by 10% from 0.2 Hz to 0.22 Hz. The resulting peak moves with the changing frequency. A close scrutiny of the peak reveals that the spikes are really the motion frequency appearing symmetrically as sidebands centered at the expected location of the non-linearity peak, as shown in Fig. 19. This strongly suggests that the noise and the sharp corners of the triangular wave is the responsible element in producing a wide hump out of the relatively sharp systematic error peak.

To see the peak clearly, it has been suggested<sup>8</sup> that the motion is encoded not with the clock timing signal, but with one of the gauge outputs and use only the sides of the triangular-wave away from the corners.

The author has chosen to encode the motion with the average of the two gauge outputs. This results in a non-uniformly sampled gauge output. A fine interpolation scheme coupled with an FFT is used by the author to rectify this problem as DFT does not work well in this case. Fig. 19 shows the resultant spatial spectrum averaged over the 24 edges of a particular triangular-wave recording. The peak appears at the expected location which is only a function of the wavelength of light in this plot. The systematic error per gauge is about 25  $\mu\text{m}$  rms. This error can be reduced further by cyclic averaging.<sup>7</sup>

First thing to note is the finite width of the peak. It is still not a spike, and in fact, it should have been. In order to resolve this problem, all 24 of the edges of the triangular wave motion in the same run is used to produce a very detailed spatial frequency spectrum. This is accomplished by “unfolding” the motion. The resultant peak is shown in Fig. 20. It is centered correctly at the right spatial frequency, but it is shattered. This is in complete accordance with the author’s expectation that the shattering and spreading are caused by the atmospheric noise in the gauge coupled to the sharp triangular corner in the motion. Two ways to resolve this experimentally are to put the whole test set-up in vacuum and repeat the experiment or to make a very linear and very large excursion path-length modulator (1 mm stroke) which only needs a very long ramp with no sharp return corners.

This part of the Keck differential phase experiment does not need vacuum. Hence, the gauge is not built to go into vacuum from the start. The large excursion path-length modulator is not needed either and it is expensive to build. To resolve this sole remaining problem, the author has written complete gauge simulator with the exact gauge outputs and systematic and random errors simulated.

Using the simulator, it has been determined that noise-free gauges with a long-stroke path-length modulator will indeed produce a sharp systematic error peak at the expected spatial frequency with the motion encoding.

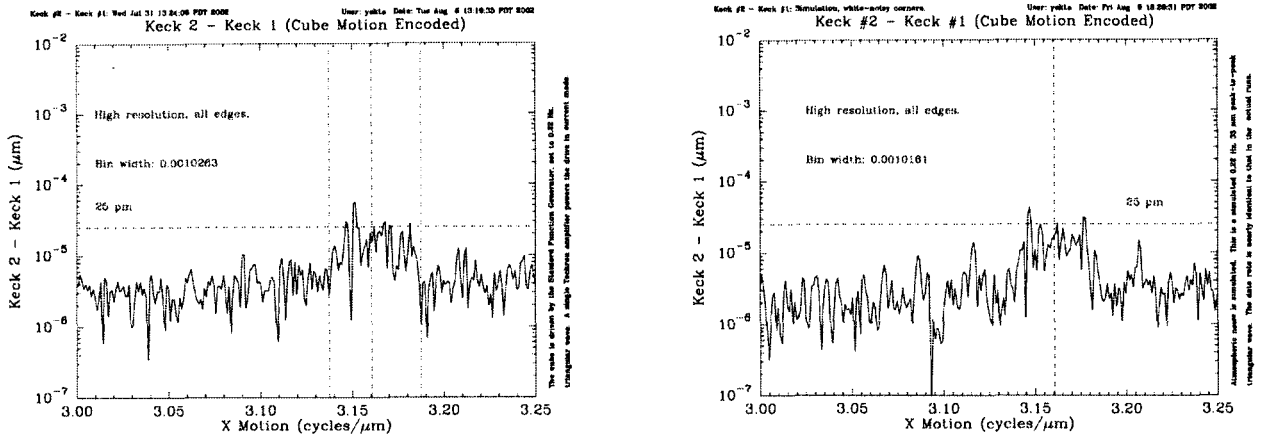


**Figure 20.** Left: The systematic error peak in the spatial domain with high-resolution resulting from motion-unfolding. Right: The simulated gauge difference output with high-frequency noise at the sharp triangular-wave motion corners.

Making the path triangular-wave, but noise-free merely displaces the peak from the expected location and widens it very slightly. Adding low frequency noise (atmospheric or other) induces more random displacements. The real cause of the shattering is the high-frequency noise right at the sharp corner of the triangular-wave motion which makes the determination of the sharp corner location impossible. Adding a few-nm-rms noise digital noise at the sharp corners of the motion, resulted in the detailed simulator output as shown in Fig. 20. The spectrum nearly identical to that out of the actual experiment with no data shared between them.

## 5. CONCLUSION

Keck differential-phase planet-detection system requires a picometer accuracy, large ( $2 \mu\text{m}$  to  $4 \mu\text{m}$ ) amplitude optical path-length modulator that can operate at fairly high frequencies (250 Hz, 750 Hz, and 1250 Hz, a partial, triangular wave motion).

We have developed a gauge which monitors the amplitude of the motion of the path-length modulator and which is capable of reaching a sensitivity of at least 3 pm per sqrt(Hz) within a band width of 1 Hz at 250 Hz, 750 Hz, and 1250 Hz. Two of these gauges are built. The gauges are compared to each other while monitoring a common optical path-length modulator to determine their accuracy. The systematic error per gauge is about 25 pm rms. This error can be reduced further by cyclic averaging.<sup>7</sup>

It is worthwhile to indicate that the Keck differential phase measurement is an AC coupled, synchronous measurement at 250 Hz, 750 Hz, and 1250 Hz in a 1 Hz bandwidth. The systematic error appears at a different frequency from these frequencies of interest. Under normal operating conditions, it will appear at a frequency higher than the highest frequency of interest (1250 Hz), and it does not effect any of the measurements as shown in Fig. 15. The systematic error is a concern only in DC measurements or in very wide-band AC measurements, like those needed by SIM.<sup>4</sup>

## ACKNOWLEDGMENTS

I would like to thank M. Shao and M.M. Colavita for many fruitful discussions. The modulator driver with the voice coils, stainless steel membranes and the cube-to-modulator mount were designed by J.D. Moore. D. Palmer made the early versions of the Keck post-amplifiers, which were later improved by the author to differential-phase picometer-capable specifications. J. Gregory helped in locating the documentation of the phase digitizer and in making it into a coherent document.

The research described was performed at the Jet Propulsion Laboratory, California Institute of Technology, under a contract with the National Aeronautics and Space Administration.

## REFERENCES

1. M.M. Colavita and P.L. Wizinowich, Keck Interferometer update, in *Interferometry in Optical Astronomy II, Proceedings of SPIE*, Vol. 4838, 2002
2. R.L. Akeson, M.R. Swain, and M.M. Colavita, Differential phase technique with the Keck Interferometer, in *Interferometry in Optical Astronomy, P.J. Lena and A. Quirrenbach, eds., Proceedings of SPIE*, Vol. 4006, p. 321, 2000.
3. Y. Gürsel, Metrology for spatial interferometry IV, in *Proceedings of SPIE conference on Small Spacecraft, Space Environments, and Instrumentation Technologies*, Vol. 3116, p. 12-26, 1997.
4. D.M. Stubbs, R.M. Bell, Jr., S.D. Barrett, T. Kvamme, Space interferometry mission starlight and metrology subsystems, in *Proceedings of SPIE Conference on Interferometry in Space*, Vol. 4852, 2002.
5. R.M. Bell, Jr., F. Zhao, P.G. Halverson, L.L. Ames, L.J. Dries, K. Dutta, D.F. Leary, G. Painter, M. Scott, SIM external metrology beam launcher (QP) development, in *Proceedings of SPIE Conference on Interferometry in Space*, Vol. 4852, 2002.
6. F. Zhao, R. Diaz, G.M. Kuan, N. Sigrist, Y. Beregovski, L.L. Ames, K. Dutta, Internal metrology beam launcher development for the space interferometry mission, in *Proceedings of SPIE Conference on Interferometry in Space*, Vol. 4852, 2002.
7. Y. Gürsel, Laser metrology gauges for OSI, in *Proceedings of SPIE conference on Spaceborne Interferometry*, Vol. 1947, p. 188-197, 1993.
8. M.M. Colavita, Private communication, July 2002.